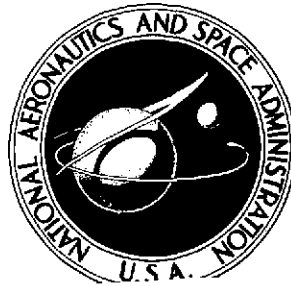


NASA TECHNICAL NOTE



NASA TN D-7483

NASA TN D-7483

(NASA-TN-D-7483) FLIGHT MONITOR FOR JET  
ENGINE DISK CRACKS AND THE USE OF  
CRITICAL LENGTH CRITERION OF FRACTURE  
MECHANICS (NASA) 21 P

N74-12187

Unclas  
H1/14 22463

IS SUBJECT TO

# FLIGHT MONITOR FOR JET ENGINE DISK CRACKS AND THE USE OF CRITICAL LENGTH CRITERION OF FRACTURE MECHANICS

*by John P. Barranger*

*Lewis Research Center  
Cleveland, Ohio 44135*

Reproduced by  
NATIONAL TECHNICAL  
INFORMATION SERVICE  
US Department of Commerce  
Springfield, VA. 22151

NATIONAL AERONAUTICS AND SPACE ADMINISTRATION • WASHINGTON, D. C. • NOVEMBER 1973

1. Report No. <b>NASA TN D-7483</b>	2. Government Accession No.	3. Recipient's Catalog No.
4. Title and Subtitle <b>FLIGHT MONITOR FOR JET ENGINE DISK CRACKS AND THE USE OF CRITICAL LENGTH CRITERION OF FRACTURE MECHANICS</b>	5. Report Date November 1973	6. Performing Organization Code
	8. Performing Organization Report No. <b>E-7570</b>	10. Work Unit No. <b>501-24</b>
7. Author(s) <b>John P. Barranger</b>	11. Contract or Grant No.	13. Type of Report and Period Covered <b>Technical Note</b>
9. Performing Organization Name and Address <b>Lewis Research Center National Aeronautics and Space Administration Cleveland, Ohio 44135</b>	12. Sponsoring Agency Name and Address <b>National Aeronautics and Space Administration Washington, D. C. 20546</b>	14. Sponsoring Agency Code
	15. Supplementary Notes	
16. Abstract  <p>A disk-crack detector is discussed which is intended to operate under flight conditions. It monitors the disk rim for surface cracks emanating from the blade root interface. An eddy-current-type sensor, with a remotely located capacitance-conductance bridge and signal analyzer, can reliably detect a simulated crack 3 mm (1/8 in.) long. The sensor was tested on a spinning turbine disk at 540° C (1000° F). Tests indicate that the system is useful at disk rim velocities to 460 m/sec (1500 ft/sec). By using fracture mechanics, it is shown for Inconel 718 that a crack operating under a rim stress of <math>34 \times 10^7 \text{ N/m}^2</math> (50 000 psi) has a critical length of 18 mm (0.72 in.).</p>		
17. Key Words (Suggested by Author(s)) <b>Nondestructive testing; Eddy current; Frac- ture mechanics; Rotors; Turbines; Compres- sors; Cracks; Cracking; Jet Engine; Frac- ture; Flight Monitor; Safety; Aircraft Safety</b>	18. Distribution Statement <b>Unclassified - unlimited</b>	
19. Security Classif. (of this report) <b>Unclassified</b>	20. Security Classif. (of this page) <b>Unclassified</b>	21. No. of Pages <b>19</b>

# FLIGHT MONITOR FOR JET ENGINE DISK CRACKS AND THE USE OF CRITICAL LENGTH CRITERION OF FRACTURE MECHANICS

by John P. Barranger  
Lewis Research Center

## SUMMARY

A disk-crack detector is discussed which is intended to operate while in flight or at the flight line. The crack detector monitors the disk rim for surface or near-surface cracks emanating from the blade root interface. The system consists of an eddy-current-type sensor and a remotely located capacitance-conductance bridge and signal analyzer.

The sensor is a coil of wire with a coil inside diameter of 3.18 millimeters (0.125 in.), an outside diameter of 9.35 millimeters (0.375 in.), and a length of 1.59 millimeters (0.062 in.). It was tested on a spinning turbine disk at rim velocities of 180 meters per second (600 ft/sec) and at 540<sup>o</sup> C (1000<sup>o</sup> F). Radial cracks in the disk were simulated by machined slits. The crack monitoring system was able to reliably detect a minimum simulated crack length of 3 millimeters (1/8 in.) under simultaneous test performance conditions of changing axial displacement, temperature cycling, and varying series capacitance.

Spin tests were also conducted on a group of disks that were removed from service because of time expiration. Cracks of the same length as the simulated crack were readily detected.

Electronically simulated transient tests indicated that the system is useful at velocities to 460 meters per second (1500 ft/sec).

Fracture mechanics is used to calculate the critical crack length. It is shown for a disk of Inconel 718 that a through-the-thickness crack operating under a rim stress of  $34 \times 10^7 \text{ N/m}^2$  (50 000 psi) has a critical length of 18 millimeters (0.72 in.). Preliminary calculations indicate that the monitoring system can provide sufficiently early warning for appropriate action to be taken.

## INTRODUCTION

Rotating parts present the most critical design and maintenance problems in an aircraft jet engine. Modes of failure depend not only on the material, but also on the operating stresses, vibration, and temperature and the environment. Compressor, fan, and turbine disks are subject to fatigue-type failures because of the cyclic nature of stresses caused by temperature and centrifugal forces. Maintenance reports indicate that radial crack propagation from the blade root area of the disk rim has been frequently encountered in service. Further, some disks are designed with abrupt changes in web thickness that result in circumferential fatigue cracks. If left undetected, these cracks can ultimately lead to catastrophic failures. Fortunately, present engine designs and inspection procedures have kept these losses to a minimum. Some commercial aircraft have added heavy containment plates to protect the aircraft and passengers should a disk separation occur. The price of the high operational reliability has been increased aircraft weight and high material and maintenance costs.

In this report, a disk-crack detector is discussed which is intended to operate while in flight or at the flight line. The crack detector monitors the disk for surface or near-surface cracks. In order to ascertain the usefulness of any disk-crack detector, it is necessary to know the critical crack length, that is, the length for which disk failure is imminent. This information can be used to determine the life remaining in the disk once the crack has been detected.

All the tests and calculations performed in this study were done in the U. S. customary system of units. The International System of Units (SI) was added for reporting purposes.

## CRACK MONITORING SYSTEM

The usual nondestructive tests for turbine disk surface cracks are the liquid penetrant, ultrasonic, and eddy current methods described in references 1 to 3. These procedures have the disadvantage that they usually require engine disassembly. The inspections, therefore, can be performed only when the engine is being overhauled.

In order to overcome this disadvantage, the disk-crack detector discussed in this report is intended to operate while in flight or at the flight line. The crack monitoring system consists of an eddy-current-type sensor, mounted approximately 1 1/2 millimeters (1/16 in.) away from the face of the disk, and the remotely located electrical capacitance-conductance bridge and signal analyzer. As the rotor spins, the disk is monitored by the sensor for surface or near-surface cracks emanating from the blade root interface. Figure 1 illustrates a typical turbine wheel segment, showing the loca-

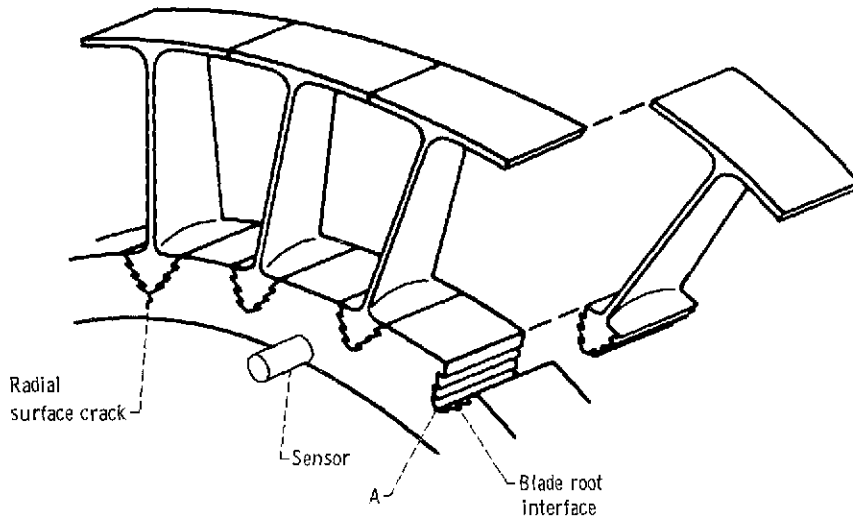


Figure 1. - Typical turbine wheel segment showing location of a radial surface crack and position of sensor.

tion of a radial surface crack and the position of the sensor. The sensor can be made an integral part of the stator or other appropriately located supporting strut.

Figure 2 is a simplified block diagram of the crack monitor. The sensor coil and cables are located inside the engine, while the automatic capacitance-conductance bridge and the crack signal analyzer are located remotely. The sensor and the bridge are connected by series capacitances and connecting cables.

The sensor is a coil of wire wound on a bobbin of glass ceramic insulator material. The coil has 60 turns of vitreous-film-insulated nickel-clad copper wire with a coil inside diameter of 3.18 millimeters (0.125 in.), an outside diameter of 9.53 millimeters (0.375 in), and a length of 1.59 millimeters (0.062 in.). The sensor can withstand operating temperatures of 540<sup>o</sup> C (1000<sup>o</sup> F), permitting its use in the high-temperature environment of the turbine section.

The sensor cables, 3.18 millimeters (0.125 in.) in diameter, pass through hollow stator blades or structural support members. The cables are made of thermocouple-type materials that can withstand inside-the-blade temperatures of 930<sup>o</sup> C (1700<sup>o</sup> F). Their resistance is about 2 ohms each for a length of 0.6 meter (2 ft).

The bridge used in the monitoring system is designed to measure capacitance and conductance. This instrument was chosen rather than the inductance-resistance type because it is the only high-frequency automatically balancing bridge that is commercially available. By adding capacitances in series with the sensor coil, the combined reactance

can be made capacitive. In figure 2, the series capacitance  $C_s$  that satisfies this condition must be such that

$$C_s < \frac{1}{2\pi^2 f^2 L}$$

where  $f$  is the bridge carrier frequency, 1 megahertz; and  $L$  is the sensor inductance. The bridge cable length is limited to about 3 3/4 meters (12 ft) because of the decreased bridge sensitivity resulting from the combination of high carrier frequency and excessive cable capacitance. For the largest commercial aircraft the cable length can be extended to 46 meters (150 ft) with the addition of transmission line matching and compensating electronics.

Eddy current devices are sensitive to temperature and displacements between the coil and the surface, as well as to all surface discontinuities. The impedance of the coil varies with temperature because of changes in the resistance of the coil and of the disk. The impedance is also influenced by the nickel-clad copper wire, which is slightly magnetic to about 370° C (700° F). The capacitance-conductance bridge is self-balancing, automatically adjusting to changes in average coil inductance and resistance caused by temperature effects and variations in disk-to-sensor spacing. The bridge has two phase detectors, one whose output voltage is proportional to the unbalanced capacitance, the other whose output is proportional to the unbalanced conductance.

The bridge takes about 1/2 second to balance, after which time the output of the conductance phase detector is monitored for out-of-balance voltages. The output of the conductance phase detector is used in the system since it is less sensitive to variations in disk-to-sensor spacing, during the monitoring time, than the capacitance phase detector. The sequence, balance then monitor, is repeated every 10 seconds. As the blade root region passes the sensor during the monitoring time, the conductance phase detector

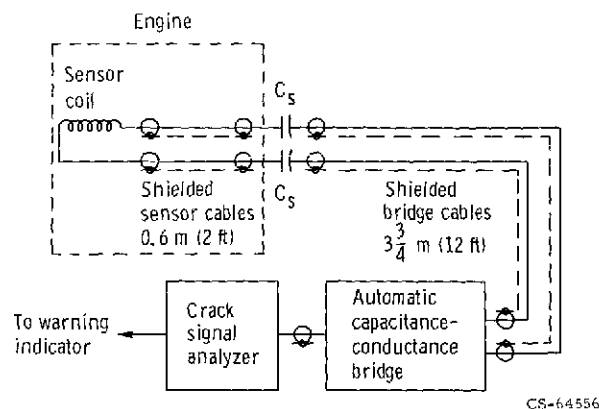


Figure 2. - Simplified block diagram of crack monitor.

senses the change in effective conductance of the sensor coil. By a process described in the next section the crack signal analyzer determines whether a crack exists and provides a signal to the warning indicator.

Fundamental to the use of the monitor is the assumption that the cracks in question occur on exposed surfaces and not under plates or bolt heads. The system, however, will detect cracks that are covered by metal a few mils thick because the eddy currents penetrate several mils into the disk surface.

With a properly located sensor the present crack monitor can detect circumferential cracks. Further, the system could be adapted to detect broken or missing blades on the turbine wheel.

### SPIN TESTS

The system has been evaluated on a spinning turbine disk. A helicopter T53 turbine wheel with simulated root cracks has been tested at speeds to 17 500 rpm, which is just under its normal operating speed. This speed is equivalent to a linear velocity under the sensor of 180 meters per second (600 ft/sec). Radial surface cracks were simulated by machined slits 0.2 millimeter (7 mil) wide and varying in length from 1 1/2 to 5 millimeters (1/16 to 3/16 in.). With the blades removed, the slits were cut from the corner marked A in figure 1, resulting in a slit having a right triangular shape with the slit length along the face of the disk approximately equal to the slit length across the thickness.

Figure 3 is a typical oscillogram of the output voltage of the conductance phase detector during the monitoring time, with the disk spinning. The oscillogram was taken at 5000 rpm but is typical of all test speeds. The base-line ripple is the blade root interface signal caused by the discontinuity in the rim region between the blade root and the disk. The pulse in the middle is the crack signal. Since the amplitude of the base-line

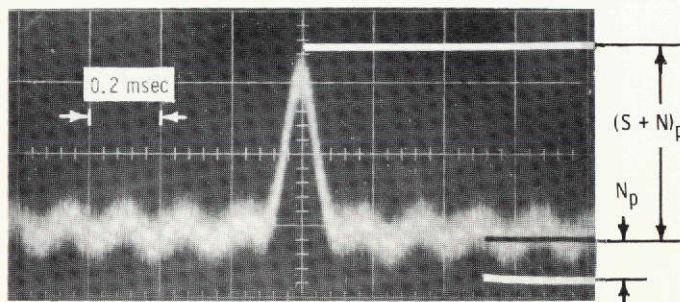


Figure 3. - Conductance voltage of automatic capacitance-conductance bridge with disk spinning, for a crack length of 3 millimeters (1/8 in.).

ripple and the crack signal vary with temperature and disk-to-sensor spacing, the absolute levels cannot be used for crack discrimination. Instead, the crack signal analyzer (appendix A) compares the crack voltage and the noise voltage to determine whether a crack exists. As indicated in figure 3, the noise voltage  $N_p$  can be determined by measuring the negative peak amplitude of the circuit noise and blade root signal. The crack voltage  $(S + N)_p$  can be determined by measuring the positive peak voltage of the sum of the crack signal, the circuit noise, and the blade root signal. The two voltages are compared, and a crack is indicated if  $(S + N)_p > 1.3 N_p$ . The quantity 1.3, which was determined experimentally, prevents random pulses from exceeding the noise voltage  $N_p$  and causing false crack indications.

The spin tests simulated some of the conditions that might be found in a flight installation. The crack monitor was designed to operate under test conditions of changing axial displacement, temperature cycling, and varying series capacitance. The following paragraphs describe these performance tests and their results.

Variations in temperature and speed cause changes in axial clearance between a turbine rotor and its stator. Further wheel wobble at the rotor frequency can modulate this clearance. To simulate these conditions, tests were conducted at clearances of 1.0, 1.5 and 2.0 millimeters (40, 60, and 80 mils) with peak modulation of  $\pm 0.25$  millimeter ( $\pm 10$  mils) at each distance. The modulation was accomplished by vibrating the sensor in the axial direction at a frequency of 10 hertz. The choice of frequency was not critical and was based on vibrator considerations. With the present sensor, the preceding values of distance and peak modulation represent the limits that the measurement system can tolerate.

Changes in temperature in the vicinity of the wheel rim cause the sensor inductance and resistance to vary. To observe these effects, low-speed tests were performed while the sensor coil and bobbin were subjected to temperature cycling from room temperature to  $540^\circ\text{C}$  ( $1000^\circ\text{F}$ ). This maximum temperature was limited by the type of wire selected for the coil.

The series capacitance  $C_s$  was 960 picofarads for all tests. The capacitance was also varied by  $\pm 50$  picofarads to simulate changes from the nominal value caused by capacitance manufacturing tolerances and temperature changes outside the engine.

The crack monitoring system was able to detect reliably a minimum simulated crack length of 3 millimeters ( $1/8$  in) under simultaneous test performance conditions of changing axial displacement, temperature cycling, and varying series capacitance.

The disk alloy of the test turbine wheel was nonferromagnetic. Depending on a number of factors, ferromagnetic materials may enhance or degrade the crack signal. No experiments were conducted on ferromagnetic disks.

The sensor was tested at a nominal axial clearance of 1.5 millimeters (60 mils). It has been pointed out that in some engines the maximum axial excursion in the turbine

during normal flight may be as much as 2.3 millimeters (90 mils). Further, surge and maneuver deflection could add as much as 2.5 millimeters (100 mils) to this variation. To accommodate these cases the sensor would have to be mounted to a feedback-controlled actuator that would maintain the axial clearance within the test condition limits.

In some small engines the temperature of the rim region of the turbine disk is about  $760^{\circ}\text{C}$  ( $1400^{\circ}\text{F}$ ). Utilization of the monitoring system at these temperatures would require a different sensor design than the one presently used.

Spin tests were also conducted on a group of T63 helicopter disks which were removed from service because of time expiration. Under low-speed, room-temperature conditions, the crack monitor was able to detect a number of radial cracks emanating from between the integrally cast turbine blades. Cracks measuring 3 millimeters ( $1/8$  in.) long in the radial direction were readily detected.

As mentioned previously in the section CRACK MONITORING SYSTEM, the output of the conductance phase detector was used since it is less sensitive to variations in disk-to-sensor spacing than the capacitance phase detector. Appendix B describes the results of terminal admittance measurements which led to this conclusion.

### TRANSIENT RESPONSE TESTS

Transient response tests were conducted to determine the effect of wheel tangential velocity on the amplitude of the crack signal. These data supplement the information from the spin tests.

Figure 4 is a simplified block diagram of the transient test system. A 1-megahertz carrier is modulated by a signal which electronically simulates the crack passing under the sensor coil. The output of the balanced modulator is inductively coupled to the sensor coil by the crack signal coil.

Figure 5 (top trace) is an oscillogram of the output of the balanced modulator simulating a 3-millimeter- ( $1/8$ -in.-) crack signal. The modulated signal is a carrier burst having a cosine squared envelope. The conductance output of the automatic capaci-

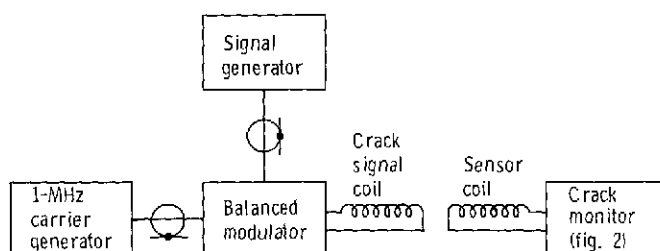


Figure 4. - Simplified block diagram of transient test system.

tance-conductance bridge is shown as the bottom trace in figure 5. Comparison of this trace and figure 3 shows that the transient response system closely approximates the crack signal obtained from the spin tests.

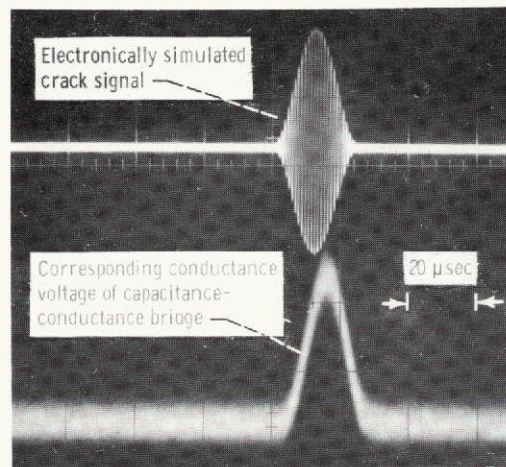


Figure 5. - Typical oscillogram of transient response tests.

In order to simulate the increase of linear velocity under the sensor, the period of the modulated signal envelope was decreased. The constant of proportionality was obtained from the spin test data. The plot of the simulated signal amplitude as a function of velocity is presented in figure 6. The amplitude is flat to 150 meters per second (500 ft/sec). At about 300 meters per second (1000 ft/sec), the maximum disk rim velocity of existing jet engines the amplitude has decreased only 5 percent. The amplitude is 10 percent lower at 460 meters per second (1500 ft/sec), the expected disk rim velocity of some future advanced engines.

The transient test data have shown that the crack monitoring system is capable of meeting the velocity requirements of current engines and will probably meet the needs of future engines.

It is sometimes useful to determine the transient response from an assumed square wave input. Figure 7 shows the square wave modulated signal and the corresponding conductance voltage. The time constant obtained from the bottom trace is about 1.5 microseconds. The transient response is limited by the capacitance-conductance bridge.

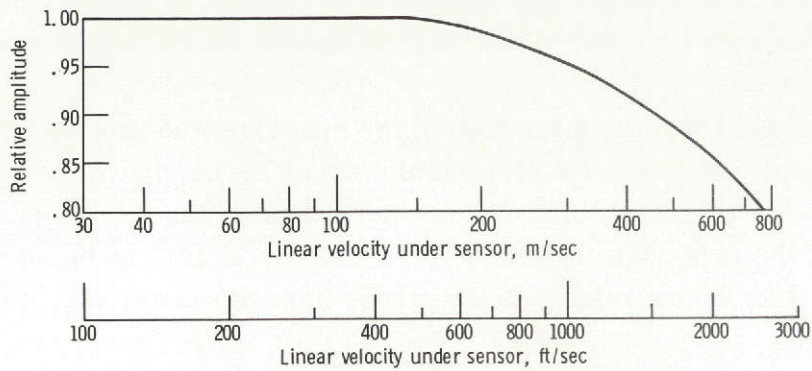


Figure 6. - Effect of disk rim velocity on simulated signal amplitude.

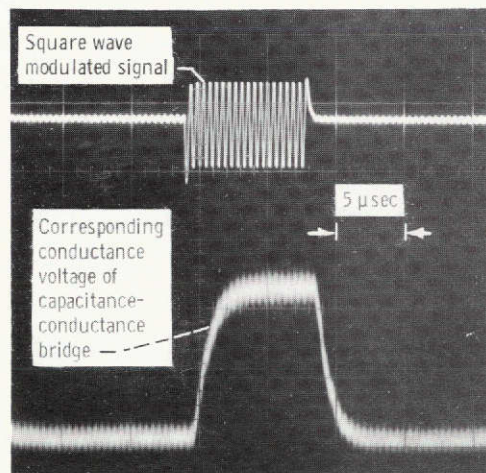


Figure 7. - Typical oscillogram of transient response from an assumed square wave input.

## CRITICAL CRACK LENGTH

In order to ascertain the usefulness of any disk-crack detector, it is necessary to know the critical length, that is, the length for which disk failure is imminent. This information, coupled with knowledge of the disk shape, material, and operating stress can be used to determine the life remaining in the disk once the crack has been detected.

A recent analytical method based on fracture mechanics (ref. 4) is used for the calculation of critical crack length. The assumption is made that crack propagation in the material can be explained by a linear elastic mechanism. In this model, yielding occurs only at the crack tip in a small plastic region. The use of this model is limited to those structures that fail in a brittle or plane strain manner. We will make this assumption

for the crack in the spinning disk. The critical crack length so calculated will be a conservative value; that is, it is shorter than any obtained from the alternate assumption of a ductile-type fracture.

The critical crack length is a function of the material, the applied tensile load, and the shape of the body. Let the tangential tensile stress at the rim of the spinning disk be designated  $\sigma$ . Further, let the radial crack extend through the thickness of the disk and let its length along the face of the disk be represented by  $a$ . It can be shown (ref 4, pp. 5 to 8) that  $\sigma$  and  $a$  are related to the stress intensity factor  $K_I$ , where

$$K_I = 1.13 \sigma(\pi a)^{1/2} \quad (1)$$

The units of  $K_I$  are  $N/m^{3/2}$  (or  $psi (in.)^{1/2}$ ).

The tangential stresses in the turbine wheel change with speed and temperature. As a result,  $\sigma$  may increase, decrease, or remain constant, with time. The crack grows in length with each stress cycle, slowly at first, until finally the change in length per cycle, called the crack growth rate, becomes large and disk separation is imminent. The crack length at the onset of rapid crack growth is the critical crack length  $a_c$ . The corresponding stress intensity factor,  $K_{Ic}$ , is called fracture toughness. Fracture toughness is a characteristic material property and is measured empirically based on methods developed by Srawley and Brown (refs. 5 and 6).

By rearranging equation (1), the critical crack length is found from

$$a_c = \frac{1}{(1.13)^2 \pi} \left( \frac{K_{Ic}}{\sigma} \right)^2 \quad (2)$$

Note that  $a_c$  is a strong function of the ratio  $K_{Ic}/\sigma$ . Any error in either of these factors will introduce large errors in  $a_c$ .

Fracture toughness and crack growth rate are not available for the test disk alloy, D-979. For a similar class of material, Inconel 718, a conservative estimate of the fracture toughness is  $93 \times 10^6 N/m^{3/2}$  ( $85\,000 psi (in.)^{1/2}$ ) (ref. 7). Assuming a maximum tangential rim stress of  $34 \times 10^7 N/m^2$  ( $50\,000 psi$ ), the critical length for these conditions is 18 millimeters ( $0.72 in.$ ). This is more than five times greater than the detectable crack length of 3 millimeters ( $1/8 in.$ ) for the test wheel monitored by the present system.

One of the important applications of fracture mechanics is the prediction of remaining life in a structure for a given crack length. Knowing the rate of crack growth allows the calculation of the number of stress cycles remaining for the detected crack to grow

to critical size. It has been found (ref. 8, p. 32) that the rate of crack growth for many materials can be represented by

$$\frac{da}{dN} = C(\Delta K_I)^n \quad (3)$$

where  $da/dN$  is the crack growth rate in units of length per cycle and  $\Delta K_I$  is the fatigue cycle range of  $K_I$ . The quantities  $C$  and  $n$  are found experimentally by testing the material under the stresses, frequency, and environment of the structure.

Combining equation (3) with (1) yields the expression

$$\frac{da}{dN} = C \left[ 1.13 \Delta\sigma(\pi a)^{1/2} \right]^n \quad (4)$$

where  $\Delta\sigma$  is the stress cycle range of  $\sigma$ . Rearranging and integrating gives

$$\int_{a_i}^{a_c} \frac{da}{a^{n/2}} = C \left[ 1.13 \Delta\sigma(\pi)^{1/2} \right]^n \int_0^{N_F} dN \quad (5)$$

where  $a_i$  is the initial crack length and  $N_F$  is the number of cycles for the crack to grow from its initial length to its critical length. Thus,  $N_F$  represents the remaining life in the structure. After integrating and rearranging, equation (5) becomes

$$N_F = \frac{a_c^{1-(n/2)} - a_i^{1-(n/2)}}{C \left( 1 - \frac{n}{2} \right) \left[ 1.13 \Delta\sigma(\pi)^{1/2} \right]^n} \quad \text{for } n \neq 2 \quad (6)$$

In a typical aircraft flight a complete temperature cycle is initiated when the engine is turned on and terminated when the engine is turned off. The initial crack length corresponds to the minimum detectable crack length of 3 millimeters (1/8 in.) for the present system. Thus, the number  $N_F$  as represented by equation (6) describes the number of flights remaining in a disk once the crack has been detected. Calculations made using preliminary data indicate that the remaining life is in excess of 100 flights, and that the monitoring system can provide sufficiently early warning for appropriate action to be taken. Because of the quantity of assumptions and approximations made in its derivation, however the results cannot be used with sufficient confidence until actual life tests are made under the true environment.

A factor which will markedly reduce the time to failure is a change in frequency or

stress level. As cracks grow, the rotor may become unbalanced, with resulting high levels of vibration. This condition will alter the magnitude of stresses and change the frequency from the engine start-stop frequency to the rotor frequency. As a consequence, the number of cycles remaining could be rapidly expended and the remaining life in terms of time could be considerably shortened.

#### CONCLUDING REMARKS

It has been shown that the disk-crack monitoring system will detect a simulated crack 3 millimeters (1/8 in.) long under conditions that might be found in a flight installation. These conditions include effects of speed, temperature, and wheel wobble.

Spin tests were also conducted on a group of disks that were removed from service because of time expiration. Cracks of the same length as the simulated crack were readily detected.

The critical crack length criterion of fracture mechanics and its remaining-life implications were reviewed. Preliminary calculations indicate that the monitoring system can provide sufficiently early warning for appropriate action to be taken.

Although tests were confined to radial surface cracks, a properly located sensor can detect circumferential cracks and could also be adapted to detect broken or missing blades on the turbine wheel.

The experimental system has not been tested in a running jet engine. The system concept remains to be evaluated under actual service conditions.

Lewis Research Center

National Aeronautics and Space Administration

Cleveland, Ohio, August 27, 1973,

501-24.

## APPENDIX A

### CRACK SIGNAL ANALYZER

The purpose of the crack signal analyzer is to provide a signal to the warning indicator when a crack exists. Figure 8 is a schematic diagram of the crack signal analyzer. The conductance voltage output of the capacitance-conductance bridge is filtered by the 160-kilohertz low-pass filter to reduce high-frequency noise. The 4-hertz high-pass filter removes the dc component of the signal.

The gain-of-10-amplifier output, designated  $S + N$  in figure 8, is applied to one of the inputs of the comparator. The voltage  $S + N$  is the sum of the crack signal, the circuit noise, and the blade root signal and has the same general appearance as the conductance voltage (fig. 3).

The gain-of-1.3 amplifier and the positive peak detector invert and produce a positive dc voltage. The output of the positive peak detector, designated  $N_p$  in figures 3 and 8, is proportional to the negative peak amplitude of the circuit noise and blade root signal.

The two voltages,  $N_p$  and  $S + N$ , are compared but will not produce a change in the output state of the comparator as long as

$$(S + N)_p < 1.3 N_p$$

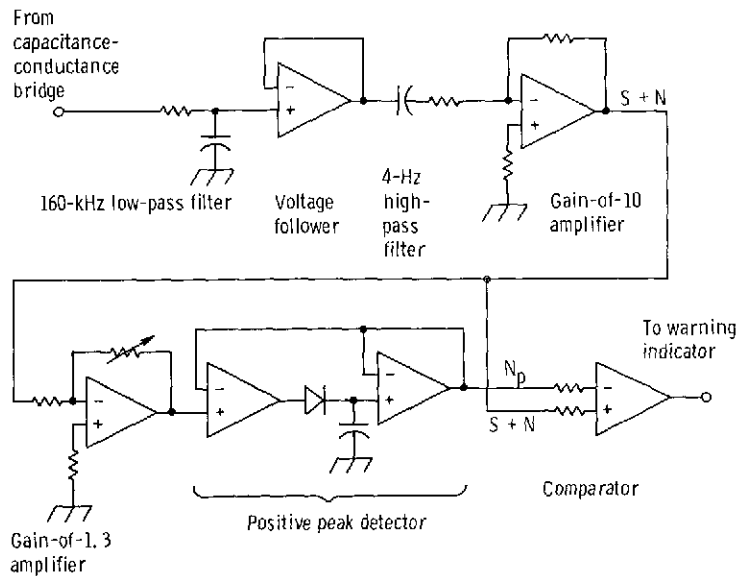


Figure 8. - Schematic diagram of crack signal analyzer.

where  $(S + N)_p$  is the positive peak value of  $S + N$ , as shown in figure 3. If, however,

$$(S + N)_p > 1.3 N_p$$

a crack is indicated and the output state of the comparator will change. The quantity 1.3, which was derived experimentally, prevents random pulses from exceeding the noise voltage  $N_p$  and causing false crack indications. An empirical determination of the value of this quantity must be made for each type of engine installation.

The output of the comparator is applied to the warning indicator. The leading and trailing edges of the comparator output signal are somewhat ragged since noise triggers the comparator when the two inputs are nearly the same in amplitude. To overcome this difficulty, the input of the warning indicator should be some kind of pulse squaring circuit, such as a monostable multivibrator.

Because of signal averaging by the high-pass filter, the voltage  $N_p$  is somewhat influenced by the number of cracks detected. In most cases, however, there are only a small number of cracks in any given disk.

## APPENDIX B

### TERMINAL ADMITTANCE

The results of terminal admittance measurements are discussed in this appendix. It is shown that the equivalent conductance output of the capacitance-conductance bridge is less sensitive to variations in disk-to-sensor spacing than the equivalent capacitance output.

The bridge terminal admittance is the admittance looking back into the sensor coil from the terminals of the automatic capacitance-conductance bridge. As shown in figure 2, the terminal admittance includes the bridge and sensor cables and the series capacitances  $C_s$ , as well as the sensor coil. At balance, the bridge display is the average value of admittance at the terminal.

Let the terminal admittance be defined by

$$Y_o = G_o + jB_o$$

where  $G_o$  is the equivalent shunt conductance,  $j$  is  $\sqrt{-1}$ , and  $B_o$  is the equivalent shunt capacitive susceptance. Figure 9 is the schematic representation of  $Y_o$ , showing the parallel combination of  $G_o$  and  $jB_o$ .

Further, let

$$B_o = \omega C_o$$

where  $\omega$  is  $2\pi$  times the frequency and  $C_o$  is the equivalent capacitance. Bridge measurements of the monitoring system yielded typical values of

$$G_o = 480 \mu\text{mhos}$$

$$C_o = 907.3 \text{ pF}$$

$$\omega C_o = 2\pi f C_o = 5698 \mu\text{mhos}$$

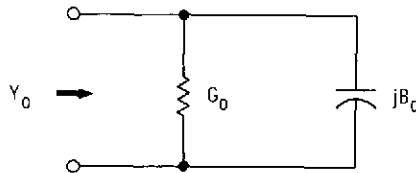


Figure 9. - Terminal admittance schematic.

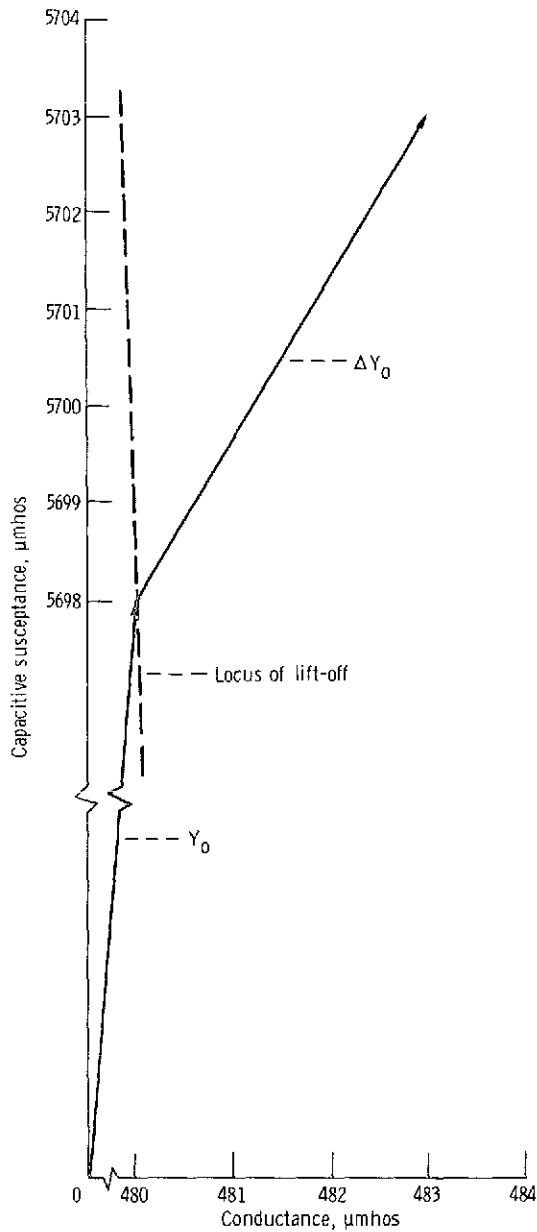


Figure 10. - Admittance diagram showing change in terminal admittance  $\Delta Y_0$ , for a 3-millimeter- (1/8-in.-) long simulated crack.

where  $f$  is the bridge carrier frequency, 1 megahertz. The bridge displays the values of  $G_0$  and  $C_0$ .

As the crack passes the sensor during the monitoring time, the sensor impedance and therefore the bridge terminal admittance change momentarily. The output of the conductance and capacitance phase detectors indicate out-of-balance voltages. Let the

corresponding change in admittance be designated by

$$\Delta Y_o = \Delta G_o + j\omega \Delta C_o$$

where  $\Delta G_o$  is the change in equivalent conductance and  $\Delta C_o$  is the change in equivalent capacitance. For a 3-millimeter- (1/8-in. -) long simulated crack, typical values are

$$\Delta G_o = 3 \mu\text{mhos}$$

$$\omega \Delta C_o = 5 \mu\text{mhos}$$

It is often instructive to picture the changes in admittance on a phasor diagram. Figure 10 is a representation of the admittances  $Y_o$  and  $\Delta Y_o$ , where the abscissa is the conductance and the ordinate is the capacitive susceptance.

Variations in disk-to-sensor spacing caused by wheel wobble change the impedance of the sensor during the monitoring time. This effect is called "lift-off." The outputs of the conductance and capacitance phase detectors are affected by lift-off. The locus of the corresponding change in admittance was experimentally determined and is shown by the dashed line in figure 10. The direction of lift-off is nearly vertical, indicating an almost purely capacitive effect. The output of the conductance phase detector is therefore less sensitive to variations in disk-to-sensor spacing than the capacitance output.

## REFERENCES

1. McMaster, Robert C. : Nondestructive Testing Handbook. Vol. II, Sections 36-42, Ronald Press, 1959.
2. Libby, Hugo L. : Introduction to Electromagnetic Nondestructive Test Methods. Wiley-Interscience, 1971.
3. Anon. : Electromagnetic Testing (for Inspection of Materiel). Quality and Reliability Assurance Handbook H 54, Office of the Assistant Secretary of Defense, Oct. 15, 1965.
4. Irwin, G. R. ; and Paris, P. C. : Fundamental Aspects of Crack Growth and Fracture. Chapter 1 in Fracture; An Advanced Treatise. Vol. III. Engineering Fundamentals and Environmental Effects, H. Liebowitz, ed. , Academic Press, 1971, pp. 1-46.
5. Srawley, John E. ; and Brown, William F. , Jr. : Fracture Toughness Testing Methods. Fracture Toughness Testing and its Applications. ASTM STP 381. American Society for Testing and Materials, 1965, pp. 133-196.
6. Srawley, John E. : Plain Strain Fracture Toughness. In Fracture; An Advanced Treatise. Vol. IV. Engineering Fracture Design, H. Liebowitz, ed. , Academic Press, 1969, pp. 45-68.
7. Popp, Herbert G. ; and Coles, Anton: Subcritical Crack Growth Criteria for Inconel 718 at Elevated Temperatures. Proceedings of the Air Force Conference on Fatigue and Fracture of Aircraft Structures and Materials: H. A. Wood, R. M. Bader, W. J. Trapp, R. F. Hoener, and R. C. Donat, eds. Rep. AFFDL-TR-70-144, Air Force Flight Dyn. Lab. (AD-719756), Sep. 1970, pp. 71-86.
8. Grosskreutz, J. C. : Fatigue Mechanisms in the Sub-Creep Range. Metal Fatigue Damage - Mechanism, Detection, Avoidance, and Repair. Manson, S: S. ed. , ASTM STP 495, American Society for Testing and Materials, 1971, pp. 5-60.